



POLITECNICO DI TORINO
Repository ISTITUZIONALE

Short-Time Transient Thermal Model Identification of Multiple Three-Phase Machines

Original

Short-Time Transient Thermal Model Identification of Multiple Three-Phase Machines / Pescetto, Paolo; Ferrari, Simone; Pellegrino, Gianmario; Carpaneto, Enrico; Boglietti, Aldo. - (2018). ((Intervento presentato al convegno IEEE Energy Conversion Congress & Exposition 2018 tenutosi a Portland, OR nel 23-27 Sept. 2018.

Availability:

This version is available at: 11583/2712414 since: 2019-07-04T17:30:14Z

Publisher:

IEEE

Published

DOI:10.1109/ECCE.2018.8557892

Terms of use:

openAccess

This article is made available under terms and conditions as specified in the corresponding bibliographic description in the repository

Publisher copyright

ieee

copyright 20xx IEEE. Personal use of this material is permitted. Permission from IEEE must be obtained for all other uses, in any current or future media, including reprinting/republishing this material for advertising or promotional purposes, creating .

(Article begins on next page)

Short-Time Transient Thermal Model Identification of Multiple Three-Phase Machines

Paolo Pescetto, Simone Ferrari, Gianmario Pellegrino, Enrico Carpaneto, and Aldo Boglietti
Dipartimento Energia Galileo Ferraris, Politecnico di Torino, Turin, Italy
paolo.pescetto@polito.it

Abstract—Short-time thermal transient identification method was successfully adopted to evaluate the slot thermal parameters of induction motors for industry applications. In this work, the modeling approach and the identification methodology are extended to the more sophisticated case of multiple three-phase machines. The generalized model takes into consideration the mutual heat exchange between the windings as well as the possible causes of temperature mismatch. A complete procedure to evaluate the parameters of the modified model is provided, supported by experimental validation on a 7.5 kW machine with two three-phase winding in contact at slot level. The method covers any type of multiple three-phase machines, whatever the thermal promiscuity of the winding sets: from deep coupling as the ones presented, to the case where only the end-turns are in contact, to the completely decoupled case. The proposed technique can be useful for the machine design and for real-time temperature monitoring during operation.

Index Terms—Thermal Model Identification; Lumped Parameters; Short-Time Transient; Multiple Winding Machines.

I. INTRODUCTION

In the past, the electrical machines design was mainly based on their electromagnetic performance requirements, but recently, the emphasis on the thermal aspects has grown, for the strong influence of the thermal behavior both on motor efficiency and reliability. This is the reason why in the last years many thermal simulation models were developed to assist the design of electrical machines [1] [2]. These models are developed according to two main approaches: Lumped Parameters Thermal-Network (LPTN) [3] or numerical methods [4]. LPTN methods provide faster response with respect to the numerical ones and can be better handled for geometry optimization during the motor design stage [5]- [7].

The extended use of motors with multiple three-phase winding systems in naval and wind applications, and more recently in aviation [8] [9] [10] has put in evidence the need of accurate thermal models capable of covering the thermal coupling among the different winding sets. The model must be valid both for steady state and transient conditions, for properly monitoring the winding conditions and preventing fault occurrence [11] [12].

This paper deals with a custom designed dual three phase winding machine prototype. The dual winding concept is an innovative technology for starter generators in aerospace application, that is expected to reduce the size of the on-board power electronic converter. This technology exploits a Permanent Magnet assisted Synchronous Reluctance (PM-SyR) machine having a stator with two sets of three-phase windings,

called primary and secondary. This is a non-conventional case of multiple three-phase machine. The two windings have different numbers of turns and wire cross sections, and so different resistance and leakage inductance. Moreover, the two three-phase sets are supplied by different currents from different converters. Every stator slot is occupied by both the sets of windings, one placed in the innermost part of each slot and the other one in the outermost. Therefore, they present different thermal behavior and strong thermal coupling, and a deep investigation of its thermal model is necessary for a full exploitation of the machine.

In this paper a lumped parameter thermal model able to represent the dynamic thermal behaviors of the two windings and their thermal coupling is presented and deeply analyzed. The procedure for the thermal parameters determination, composed by three tests, is discussed. Two mathematical approaches are proposed for the parameters computation: the first one, approximated but simple, can be used for fast evaluation of the LPTN parameters. The second one is based on an analytical approach. The two methods gave similar results.

The proposed procedure can be usefully adopted for 1) improving the accuracy of the steady-state and transient thermal estimate during the machine design, 2) building a simple and accurate transient thermal model that can be used for online temperature monitoring [13] of highly overloaded machines, or fault tolerant machines when one sector fails or for the prognostics of the windings failure in critical applications.

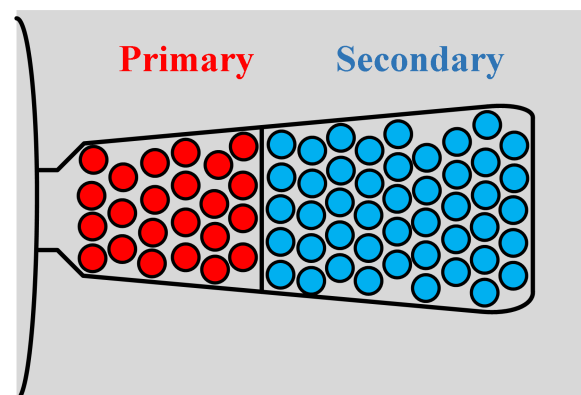


Fig. 1. Schematic of winding allocation in the slot of the DW machine.

TABLE I
DW MACHINE SPECIFICATIONS

	Primary	Secondary
Rated power [kW]		7.5
Rated speed [rpm]		3000
Rated load current [A]		40
DC link voltage [V]		270
Number of pole pairs		4
Number of slots		36
Number of turns in series per phase	30	60
Phase resistance [$m\Omega$]	194	372
Copper Mass [kg]	2.1	4.5

II. LPTN OF MULTIPLE THREE-PHASE MACHINES

The Dual Winding (DW) machine used for the experimental measurements is a 4 pole/36 slots PM-SyR machine prototype with ferrite permanent magnets. Table I reports its main parameters. Each windings set is a standard three-phase single-layer full-pitch winding. The two sets are placed in the same slots, as shown in Fig. 1, with a cross-section proportional to the number of turns of each set.

According to the requirements of the DW technology, the number of turn of the secondary winding is higher respect to the primary one, while the two three-phase sets can have different wire section, resulting in different stator resistances. If connected in series, the DW machine becomes a standard single winding machine.

A. Review of the Three-Phase Case

Previous works [11] [12] demonstrated the effectiveness of the short-time thermal transient method to identify the parameters of a LPTN of various three-phase induction motors of different size for industrial application in real operating conditions. The adopted model is shown in Fig. 2, where the current generator stands for Joule loss P_j in the winding, the capacitor C_{eq} represents the thermal capacitance of winding plus insulation and the resistor R_{eq} is the thermal resistance from the winding to the stator core iron.

Starting with the motor at room temperature T_0 , the three phases are connected in series and excited with direct current while the resistance is online monitored. The amplitude of the injected current is in the order of magnitude of the rated value. Since the initial temperature T_0 and winding resistance R_0 are known, the average winding temperature can be estimated using the well known relationship:

$$T = \frac{R_T}{R_0} \cdot (234.5 + T_0) - 234.5 \quad (1)$$

where R_T is the winding resistance at the temperature T and 234.5 is the inverse of copper temperature coefficient. According to the scheme in Fig. 2, the thermal transient is approximated by an exponential curve:

$$T(t) = T_0 + T_\infty \left(1 - e^{-\frac{t}{\tau}}\right) \quad (2)$$

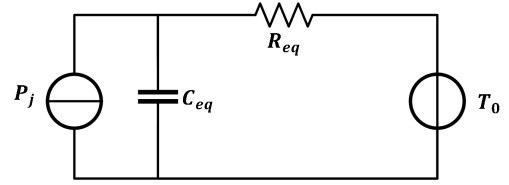


Fig. 2. LPTN for single three-phase winding machines.

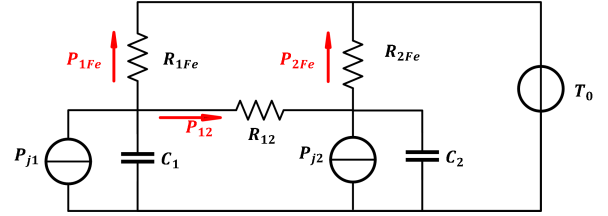


Fig. 3. LPTN for dual three-phase winding machines.

where $T_\infty = P_j R_{eq}$ and $\tau = R_{eq} C_{eq}$ is the time constant. The initial stage of the temperature transient is adiabatic, i.e. iron core temperature does not change respect to T_0 . So, the accumulated energy W versus winding temperature is almost a straight line, whose slope equals the equivalent thermal capacitance:

$$C_{eq} = \frac{dW}{dT} \quad (3)$$

After evaluating C_{eq} from (3), the equivalent resistance R_{eq} is extracted from the time constant τ evaluated in (2). Details can be found in [11] [12].

B. Multiple Three-phase Windings

The LPTN of a dual three-phase machine, and namely of the DW machine under test, is reported in Fig. 3. Each three-phase set of windings has its proper thermal capacitance, called C_1 and C_2 , aggregating the respective winding copper and insulation. Moreover, two thermal power generators P_{j1} and P_{j2} represent the respective stator Joule losses. Each winding exchanges heat with the stator iron through the thermal resistances R_{1Fe} and R_{2Fe} . Moreover, a quota of thermal power P_{12} is exchanged between the two windings, flowing through the resistance R_{12} . It must be remarked that in this specific machine the two windings share the same slots, therefore the contact surface between them is relatively high compared with other types of multiple three-phase machines adopting different slots for the different windings. For this reason, the heat exchange between the two windings is particularly significant, and the value of R_{12} is comparable with R_{1Fe} and R_{2Fe} .

In principle, the stator iron has its thermal capacitance, too. However, thanks to the adiabatic hypothesis, the iron temperature is considered constant during the first part of the transient (approximately one minute) and represented by the voltage generator T_0 . In other words, the thermal capacitance of the iron is initially considered infinite.

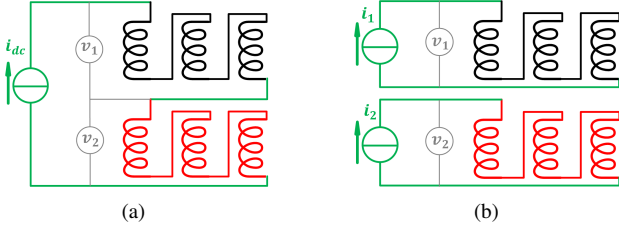


Fig. 4. Winding configuration for a) test 1 and b) test 2 and 3.

C. Test Sequence

The test procedure described in Section II-A is slightly complicated here to find the five parameters of the LPTN of Fig. 3. The three phases of each winding set are always series connected, as shown in Fig. 4. The identification procedure consists of three tests:

- 1) all windings: primary three-phase set connected in series to secondary, and excited with constant current $i_{dc} = 20$ A;
- 2) primary only: the two windings are separated and only the primary channel is excited at 20 A;
- 3) secondary only: the two windings are separated and only the secondary channel is excited at 20 A;

The 20 A excitation current is chosen of the same order of the rated current of each winding set. During the test, the dc resistances of the two windings R_1 and R_2 are online measured using the voltage measurement indicated in Fig. 4, divided by the imposed current. In the “primary only” and “secondary only” tests, a small current (1 A) is injected into the non excited winding. This current is only necessary for online monitoring the winding resistance, but it has negligible thermal effect. Based on the measured resistances, the average temperatures of the two windings are estimated:

$$T_1 = \frac{R_{1,T1}}{R_{1,0}} \cdot (234.5 + T_0) - 234.5 \quad (4a)$$

$$T_2 = \frac{R_{2,T2}}{R_{2,0}} \cdot (234.5 + T_0) - 234.5 \quad (4b)$$

where $R_{1,T1}$ and $R_{2,T2}$ are the two resistances at the temperatures T_1 and T_2 and $R_{1,0}$ and $R_{2,0}$ are the resistances at the initial temperature T_0 . The thermal energy dissipated in the two windings is calculated from the electric power:

$$W_1 = \int v_1 \cdot i_1 dt \quad (5a)$$

$$W_2 = \int v_2 \cdot i_2 dt \quad (5b)$$

D. Rapid Data Manipulation: test 1

After measuring the thermal transient, the parameters of the equivalent LPTN are obtained via data manipulation. In the first test (“all windings”), the two windings present similar power loss density and their temperature rises are similar. For this reason, it is assumed that the thermal energy exchange P_{12}

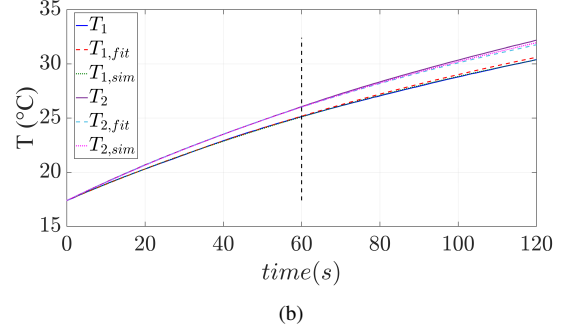
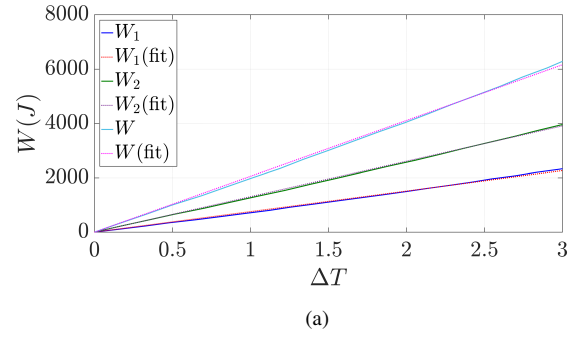


Fig. 5. (a) Energy Vs overtemperature and (b) temperature transient in the test 1 (series connection). Solid lines: measured data. Dashed: interpolation based on the first 60 seconds using (9) and (10). Dotted: simulation with LPTN in Fig. 3.

between the two windings can be neglected, so the thermal network is simplified as in Fig. 8(a).

$$P_{12} = 0 \quad (6)$$

By using this simplified model, the windings are decoupled and separately studied as two independent single winding machines. Therefore, the same procedure described in Section II-A is adopted to evaluate R_{1Fe} , R_{2Fe} , C_1 and C_2 . The thermal capacitances are obtained from the slope of the dissipated energy as a function of the overtemperature approximated with a straight line, while the resistances are calculated from the time constants of the fitting exponential functions:

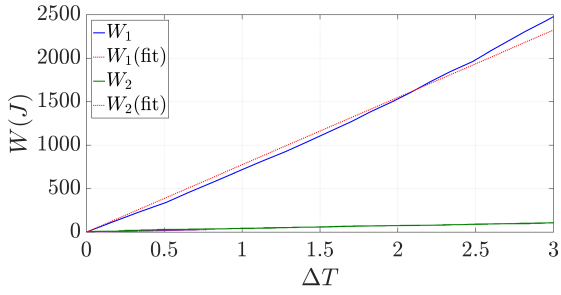
$$C_1 = \frac{dW_1}{dT_1} \quad (7)$$

$$C_2 = \frac{dW_2}{dT_2} \quad (8)$$

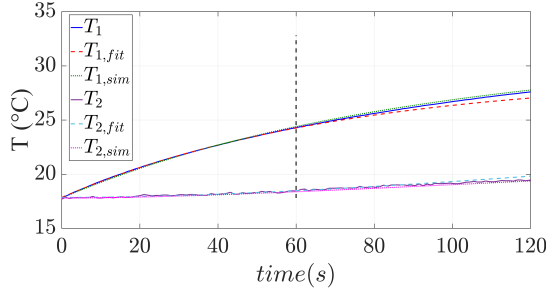
$$T_1(t) = T_0 + \Delta T_{1,\infty} \left(1 - e^{-\frac{t}{\tau_1}}\right) \quad (9)$$

$$T_2(t) = T_0 + \Delta T_{2,\infty} \left(1 - e^{-\frac{t}{\tau_2}}\right) \quad (10)$$

where $\Delta T_{1,\infty} = P_{j1}R_{1Fe}$, $\Delta T_{2,\infty} = P_{j2}R_{2Fe}$, $\tau_1 = R_{1Fe}C_1$ and $\tau_2 = R_{2Fe}C_2$.



(a)



(b)

Fig. 6. (a) Energy Vs overtemperature and (b) temperature transient in the test 2 (primary only). Solid lines: measured. Dashed: interpolation based on the first 60 seconds using (14) and (18). Dotted: simulation with LPTN in Fig. 3.

E. Rapid Data Manipulation: test 2 and 3

In the second test (“primary only”), the temperature of the secondary winding varies by less than 1 °C respect to the initial room temperature. Therefore the heat exchange between the secondary coil and the iron is negligible. Moreover, it is considered that the power loss in the secondary winding is null:

$$P_{j2} = 0 \quad (11)$$

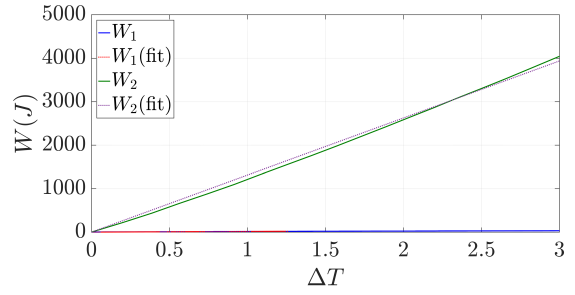
The LPTN is then simplified as in Fig. 8(b). It must be remarked once more that this analysis is valid only in the initial part of the thermal transient, when adiabatic condition holds (60 seconds). Using the simplified circuit, the power flow between the two windings is:

$$P_{12} = C_2 \frac{dT_2}{dt} \quad (12)$$

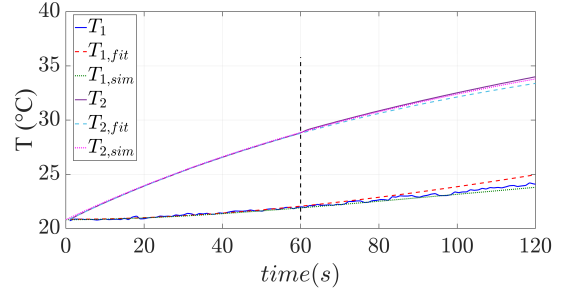
where C_2 is known from the first test. The mutual exchange thermal resistance R_{12} is calculated after the exchanged power P_{12} , as:

$$R_{12} = \frac{T_1 - T_2}{P_{12}} \quad (13)$$

It must be noted that T_1 , T_2 and P_{12} are a function of time, therefore a variable R_{12} is found through (13). Anyway, the thermal system is linear, so the value of R_{12} changes very little and it can be reasonably considered as constant. The average of R_{12} in the first 60 s is reported in Table II.



(a)



(b)

Fig. 7. (a) Energy Vs overtemperature and (b) temperature transient in the test 3 (secondary only). Solid lines: measured data. Dashed: interpolation based on the first 60 seconds using (14) and (18). Dotted: simulation with LPTN in Fig. 3.

Different hypothesis are separately adopted to find an analytical expression of T_1 and T_2 . According to the LPTN of Fig. 8(b) if the temperature variation of the secondary winding is neglected, T_1 follows a first order exponential transient:

$$T_1 = T_0 + \Delta T'_{1,\infty} \left(1 - e^{-\frac{t}{\tau'_1}} \right) \quad (14)$$

where $\Delta T'_{1,\infty} = P_{j1} R_{1,eq}$, $\tau'_1 = C_1 R_{1,eq}$ and $R_{1,eq} = R_{12} \parallel R_{1,Fe}$. The advantage of this formulation is that it is suitable for numeric optimization, since P_{j1} is measured and $R_{1,Fe}$ and C_1 are known from the test “all windings”. Therefore, an alternative estimation of R_{12} can be obtained and compared with (13). This approach is under investigation at the moment of this work.

After calculating T_1 through (14), different hypothesis are adopted to find an analytical expression of T_2 . In this case, the primary winding is seen as a current generator providing the thermal power P_{12} . Therefore, the temperature in the secondary winding is approximated as:

$$T_2 = T_0 + \frac{1}{C_2} \int_0^t P_{12} dt \quad (15)$$

From (13) and (14):

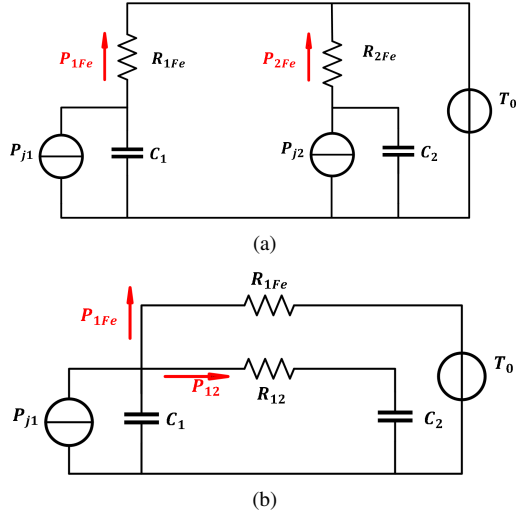


Fig. 8. LPTN in the test where (a) the winding are series connected and (b) primary winding only is excited.

$$T_2 = T_0 + \frac{1}{C_2} \int_0^t \frac{T_1 - T_2}{R_{12}} dt \quad (16)$$

$$\approx T_0 + \frac{1}{C_2 R_{12}} \int_0^t \Delta T'_{1,\infty} \left(1 - e^{-\frac{t}{\tau_e}}\right) dt \quad (17)$$

By solving (17), an analytical approximated expression is obtained for T_2 :

$$T_2 = T_0 + \frac{P_{j1} R_{1,eq}}{C_2 R_{12}} \left(t + \tau'_1 e^{-\frac{t}{\tau'_1}} - \tau'_1 \right) \quad (18)$$

As said, T_2 is measured via R_2 , using a small current value (1 A). As a consequence, T_2 is noisy, significantly affecting the derivative in (12). Therefore, it may be necessary to preliminary filter the measured temperatures. Alternatively, an analytical expression of T_2 derivative can be conveniently obtained from (18), assuming constant Joule losses P_{j1} :

$$\frac{dT_2}{dt} = \frac{P_{j1} R_{1,eq}}{C_2 R_{12}} \left(1 + e^{-\frac{t}{\tau'_1}} \right) \quad (19)$$

Finally, the “secondary only” test follows the same steps of the latter one. Under the same hypothesis, R_{12} is calculated again. The good match of R_{12} estimates from the two tests, report in Table II, proofs the consistency of the test sequence. The two estimates differ for less than 5 %, which is considered acceptable for most of the LPTN applications.

F. Formal approach to data manipulation

A feasible alternative to the procedure described in II-D and II-E is to analytically solve the LPTN of Fig. 3. With constant winding currents, the variation of thermal power due to the dependence of the electrical resistance on the temperature can be modeled with a Norton equivalent circuit, with constant thermal power in parallel to a negative thermal resistance [12]. The negative resistances are required to take into account the increase of dissipated power on varying the winding resistance.

In this way, the input of the system becomes a step function, and the admittance matrix can be written in Laplace domain to analytically solve the LPTN.

Basing on the analytical solution it is possible to predict the winding temperature for a given parameters set. The three tests present the same analytical solution, and differ one from the other only for the amplitude of input thermal power. The aggregate root mean square error $RMSE$ between measured and predicted temperatures in the three tests is calculated as:

$$RMSE = \sqrt{\frac{\sum_{p=1}^3 (\hat{T}_1 - T_1)^2 + \sum_{p=1}^3 (\hat{T}_2 - T_2)^2}{2 \sum_{p=1}^3 (N_p - 1)}} \quad (20)$$

where \hat{T}_1 and \hat{T}_2 are the predicted winding temperatures, p is the index of the test and N_p the number of measurement point for a given test. A Nelder-Mead derivative-free optimization algorithm was used to minimize the $RMSE$ calculated in (20), obtaining the parameters set report in Table III [14].

As can be noticed, the two proposed methods gave compatible results, and the discrepancy between them is acceptable for the practical application of LPTN. The advantage of the formal approach is that it permits to easily extended the model to an n^{th} order system, e.g. to take into account finite iron thermal capacitance.

III. EXPERIMENTAL RESULTS

The thermal model identification procedure was experimentally tested on the DW machine described in Section II. The experimental set-up is simple and it only requires two dc current sources, two current and two voltage probes. HBM Gen7i having 18 bit, 0.01% class voltage channels associated to 0.1% class current probes was used.

It is considered that the hypothesis of short transient operation (e. g. adiabatic conditions) hold up to 60 s. A sufficiently high time range is desirable in order to have a high number of measurement points to be used in the curve fitting and parameters estimation. Conversely, if a too long time limit is chosen the adiabatic conditions fall and the thermal transient can not be well approximated with a first order exponential. The time window limit was chosen basing on the energy Vs overtemperature plot: when adiabatic conditions fall the curve is not anymore represented by a straight line.

Using the obtained parameters, the thermal network of Fig. 3 was implemented using Matlab-Simulink. The three tests were simulated imposing the correspondent power loss, and the obtained temperatures were plotted in Fig. 5(b), 6(b) and 7(b) (dotted lines). As can be seen the agreement with the measured temperatures is very good in all the tests. The maximum discrepancy between measured and predicted temperatures up to 120 s is around 1%. For the test “all windings”, the discrepancy between the measured and predicted overtemperatures in the two windings are bounded between -0.15 and 0.23 °C in the first 180 s of test. In the same time range, the temperature discrepancies for the test “primary

TABLE II

LPTN PARAMETERS ESTIMATED WITH RAPID DATA MANIPULATION.

C_1	C_2	R_{1Fe}	R_{2Fe}	R_{12} from test 2	R_{12} from test 3
J/°C	J/°C	°C/W	°C/W	°C/W	°C/W
765	1313	0.191	0.131	0.260	0.248

only” were limited between -0.28 and 0.32 °C, and for the test “secondary only” between -0.09 and 0.57 °C. In conclusion, the LPTN with the calculated parameters matches very well with the measurement results.

The same figures also show the temperature transient interpolated with analytical fitting functions based on the first 60 s. The interpolating functions are (9) and (10) for the test series, while for the test primary the fitting functions are (14), (18). As can be seen, the complete model of figure 3 is more accurate, especially after the time frame of 60 s.

IV. CONCLUSION

The characterization of the copper to iron thermal model based on short-time thermal transient identification, already presented for three-phase motors, was successfully extended to multiple three-phase machines. A new lumped parameters thermal model is proposed and validated. This model is valid for an arbitrary number of stator windings and it can be



Fig. 9. Experimental setup: dual winding machine, DC power supplies and HBM Gen7i data logger.

TABLE III

LPTN PARAMETERS ESTIMATED WITH THE FORMAL APPROACH.

C_1	C_2	R_{1Fe}	R_{2Fe}	R_{12}
J/°C	J/°C	°C/W	°C/W	°C/W
793	1325	0.208	0.146	0.218

easily applied to any multi-phase machine. Moreover, it can be extended to include finite iron capacitance, increasing the degree of freedom of the thermal network. The test procedure, together with two methods for calculating the parameters of the analytical model where presented and validated on a 7.5 kW dual winding machine prototype. The two post-processing approaches gave compatible results. The proposed model and identification procedure can be usefully adopted for real-time temperature monitoring in critical applications, and as a valid support to the design of multiple three-phase machines.

REFERENCES

- [1] P. H. Mellor, D. Roberts and D. R. Turner, “Lumped parameter thermal model for electrical machines of TEFC design,” in *IEEE Proceedings B - Electric Power Applications*, vol. 138, no. 5, pp. 205-218, Sept. 1991.
- [2] A. Boglietti, A. Cavagnino, D. Staton, M. Shanel, M. Mueller, C. Mejuto, “Evolution and Modern Approaches for Thermal Analysis of Electrical Machines” *IEEE Trans. Ind. Elec.* Vol. 56, no.3, March 2009.
- [3] A. Boglietti, A. Cavagnino, M. Lazzari and M. Pastorelli, “A simplified thermal model for variable-speed self-cooled industrial induction motor,” in *IEEE Transactions on Industry Applications*, vol. 39, no. 4, pp. 945-952, July-Aug. 2003.
- [4] W. Jiang, T. M. Jahns, “Coupled Electromagnetic–Thermal Analysis of Electric Machines Including Transient Operation Based on Finite-Element Techniques,” in *IEEE Transactions on Industry Applications*, vol. 51, no. 2, pp. 1880-1889, March-April 2015.
- [5] C. Kral, A. Haumer and S. B. Lee, “A Practical Thermal Model for the Estimation of Permanent Magnet and Stator Winding Temperatures,” in *IEEE Transactions on Power Electronics*, vol. 29, no. 1, pp. 455-464, Jan. 2014.
- [6] N. Simpson, R. Wrobel and P. H. Mellor, “Estimation of Equivalent Thermal Parameters of Impregnated Electrical Windings,” in *IEEE Transactions on Industry Applications*, vol. 49, no. 6, pp. 2505-2515, Nov.-Dec. 2013.
- [7] Y. Bertin, E. Videcoq, S. Thieblin and D. Petit, “Thermal behavior of an electrical motor through a reduced model,” in *IEEE Transactions on Energy Conversion*, vol. 15, no. 2, pp. 129-134, Jun 2000.
- [8] R. Bojoi, M. G. Neacsu and A. Tenconi, “Analysis and survey of multi-phase power electronic converter topologies for the more electric aircraft applications,” *Int. Symposium on Power Electronics, Electrical Drives, Automation and Motion*, Sorrento, 2012.
- [9] E. Levi, “Multiphase Electric Machines for Variable-Speed Applications,” in *IEEE Transactions on Industrial Electronics*, vol. 55, no. 5, pp. 1893-1909, May 2008.
- [10] M. Villani, M. Tursini, G. Fabri and L. Castellini, “Multi-phase fault tolerant drives for aircraft applications,” *Electrical Systems for Aircraft, Railway and Ship Propulsion*, Bologna, 2010, pp. 1-6.
- [11] T. Huber, W. Peters and J. Böcker, “A low-order thermal model for monitoring temperatures in permanent magnet synchronous motors,” *7th IET International Conference on Power Electronics, Machines and Drives (PEMD 2014)*, Manchester, 2014, pp. 1-6.
- [12] A. Boglietti; E. Carpaneto; M. Cossale; S. Vaschetto, “Stator-Winding Thermal Models for Short-Time Thermal Transients: Definition and Validation”, *IEEE Trans. on Industrial Electronics*, 2016.
- [13] N. Jaljal, J. F. Trigeol and P. Lagonotte, “Reduced Thermal Model of an Induction Machine for Real-Time Thermal Monitoring,” in *IEEE Transactions on Industrial Electronics*, vol. 55, no. 10, pp. 3535-3542, Oct. 2008.

- [14] Pérez-Arriaga I. J., Verghese G. C., Schweppe F. C., "Selective Modal Analysis with Applications to Electric Power Systems. Part 1: Heuristic Introduction", *IEEE Transactions on Power Apparatus and Systems*, Vol. PAS-101, No. 9, September 1982, pp. 3117-3125